THE JOURNAL OF PHYSICAL CHEMISTRY A

ARTICLE

pubs.acs.org/JPCA

Combined SPR and SERS Microscopy in the Kretschmann Configuration

Stefan A. Meyer, Baptiste Auguié, Eric C. Le Ru, and Pablo G. Etchegoin*

The MacDiarmid Institute for Advanced Materials and Nanotechnology, School of Chemical and Physical Sciences, Victoria University of Wellington, P.O. Box 600, 6140 Wellington, New Zealand

Supporting Information

ABSTRACT: A novel hybrid spectroscopic technique is proposed, combining surface plasmon resonance (SPR) with surface-enhanced Raman scattering (SERS) microscopy. A standard Raman microscope is modified to accommodate the excitation of surface plasmon-polaritons (SPPs) on flat metallic surfaces in the Kretschmann configuration, while retaining the capabilities of Raman microscopy. The excitation of SPPs is performed as in standard SPR-microscopy; namely, a beam with TM-polarization traverses off-axis a high numerical aperture oil immersion objective, illuminating at an angle the metallic film from the (glass) substrate side. The same objective is used to collect the full Kretschmann cone containing the SERS emission on the substrate side. The angular dispersion of the plasmon resonance is measured in reflectivity for different coupling conditions and, simultaneously, SERS spectra are recorded from Nile Blue (NB) molecules adsorbed onto the surface. A trade-off is identified between the conditions of optimum coupling to SPPs and the spot size (which is related to the spatial resolution). This technique opens new horizons for SERS microscopy with uniform enhancement on flat surfaces.

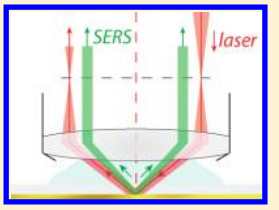

INTRODUCTION AND OVERVIEW

In the past few years, a fast-growing interest in surface-enhanced Raman scattering (SERS)[1,2] has led to the development of a vast range of different possible substrates.[3−10] Fabrication techniques ranging from colloidal chemistry[11−13] to nanolithography[5,14] have been explored, featuring increasingly elaborate designs of nanostructures to harness the incident light and optimize its interaction with Raman-active molecules. Indeed, it is generally a combination of geometrical factors and the specific metal/dielectric materials used for a SERS substrate that enables the highest reported enhancements, such as in the gap between particles,[13,15] at the sharp tip of nanoparticles,[16] or the two acting in concert.[17−19] The emerging field of plasmonics[20−22] has hitherto provided a playground for experimental and computational studies aiming at optimizing the local field enhancement in the proximity of metal nanostructures. While the optimization of the Raman enhancement factor[23] has enabled single-molecule detection in a wide variety of cases,[24−32] and there is an increasing number of studies claiming reproducibility,[13,33] such substrates still suffer from spatial inhomogeneities in their enhancements. After decades of research, the fact still remains that, the higher the SERS enhancement, the more uncontrollable it becomes (dubbed informally the "SERS uncertainty principle"[34]). The emphasis in the search for high enhancements for single-molecule SERS applications has perhaps left a gap in the more applied pursuits of analytical Raman spectroscopy.[35] Our paper here fits in that gap left in the application of SERS for analytical purposes. We aim at developing a new technique for performing SERS with uniform enhancement and with the added ingredient of microscopy.

Motivation: A Shift in Paradigm for SERS Substrates. The bewildering variety of studied substrates has provided a wide-ranging framework within which the SERS effect can be studied with many different variations to explore its subtle aspects. Notwithstanding the necessity of such pursuits, it should be recognized that this diversity can sometimes come as a disadvantage: unless a substrate displays a truly revolutionary new property over previous realizations, its impact is diluted in the pool of possibilities. It is not uncommon to see new SERS substrates being pursued only by isolated efforts or to be abandoned altogether over time. This situation is further aggravated by problems of reproducibility and highly specialized experimental conditions that are difficult or cumbersome to replicate. In that context, a return to simpler substrates (such as planar metallic films) with improved experimental tools that enhance the capabilities of SERS is an appealing option for many applications.[35] Substrates with lower (but reproducible) enhancements have been developed for commercial applications of SERS in bioanalytical and forensic sciences.[5,36,37] Relatively uniform enhancements of $\sim 10^3$ (up to $\sim 10^5$ for thiolated compounds) have been quoted in this context. One should note also that enhancements of the order of $\sim 10^3$ represent only a superficial limitation, for SERS outperforms many analytical tools even in this range. Furthermore, enhancement factors of $\sim 10^3$ may, in principle, be enough to be able to detect single *resonant* molecules (with intrinsic cross sections of the order of $\sim 10^{-24}$ cm^2/sr[38,39]). Hence, there is a clear drive to pursue the study of substrates with well-controlled uniform SERS enhancements over large areas.[35]

Received: November 8, 2011
Revised: December 18, 2011
Published: December 19, 2011

Unlike the vast majority of work done on SERS substrates in the past few years, the important developments presented in this paper are *not* in the nanotechnology or chemistry of the SERS substrate, but rather in the way the signal is coupled to, detected from, and spatially resolved in (arguably) the simplest plasmonic system: a flat gold surface. Planar thin metal films offer several distinct advantages over their more fashionable siblings such as nanoparticles, nanoholes, rough surfaces, gratings, and so on. First, planar layers of high quality and uniformity are readily manufactured; they are in fact commonly available for commercial applications of surface plasmon resonance (SPR) sensing and spectroscopy. Second, the field enhancement resulting from the excitation of propagating surface plasmon-polaritons (SPPs) is highly uniform over large areas, albeit with weaker field confinement and enhancement than its localized plasmon counterpart found in nanostructures. In addition, the well-established theoretical treatment of planar surfaces, by rigorous analytical solution of Maxwell's equations, enables accurate comparisons between theory and experiments. Last, but not least, there are fundamental aspects of the SERS effect that can most effectively be pursued on planar surfaces (due to the simplicity of the interpretation), such as that of surface-selection rules[40,41] or the often elusive (difficult to quantify) contribution of a chemical enhancement factor in SERS.[42]

Combining SPR and SERS Spectroscopy. The excitation of SPPs in the Kretschmann configuration is the basis of SPR (bio)sensing, a widely used and mature surface characterization technique that provides excellent sensitivity (albeit with little specificity) to minute changes of composition in the vicinity of a metal substrate;[45−51] as such, it offers a very convenient and easily parallelized platform with industrial applications. Likewise, the Raman spectrum of known molecules in SERS can be used to identify unambiguously the chemical composition of trace amounts of material.[5,36,37] It is obvious that these two techniques can complement each other to provide rapid and quantitative detection (with uniform enhancement) of unknown analytes binding to a gold substrate. Only few attempts have been reported in the literature to perform SERS measurements in the Kretschmann configuration (see ref 35 for an overview of previous work). Because of the sharp angular dependence of the coupling to SPPs, the excitation and collection of SERS signals in the Kretschmann configuration require a number of special considerations compared to "standard" SERS experiments. In particular,[35] efficient coupling to SPPs in excitation requires a highly collimated (nondivergent) exciting beam. Moreover, the SERS signal is primarily emitted on the prism side within a narrow angular cone: the Kretschmann cone. These two major aspects are further illustrated in the theoretical predictions shown in Figure 1. The moderate ($\sim 10^2$-fold for the perpendicular configuration) enhancement of the electromagnetic field provided by the SPP resonance benefits the SERS signal in two ways. First, as the incident light couples to the resonance, the Raman probe experiences an enhanced excitation; second, by virtue of reciprocity,[44] light emission at the Raman frequency is also enhanced in the same fashion, but only in this particular direction (hence, the appearance of a Kretschmann cone for the emitted light). The calculation suggests that SERS enhancement factors (EFs) of up to $\sim 10^4$, as estimated[44] by $|E_{Loc}|^4/|E_0|^4$, are theoretically possible. This figure should, however, be taken with a loose interpretation because (unlike what happens in the vast majority of other SERS experiments) the actual enhancement of the SERS signal crucially depends on the excitation and collection optics

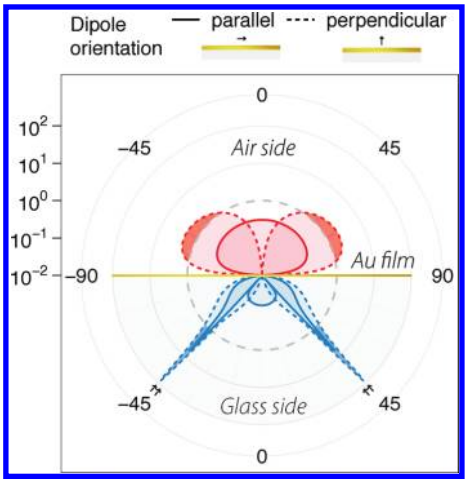

Figure 1. Theoretical radial pattern (in log-polar coordinates) for the local field intensity enhancement factor at $\lambda = 632.8$ nm experienced by a parallel (solid lines) or perpendicular (dashed lines) dipole situated 1 nm above a 50 nm gold layer[43] supported by a semi-infinite glass substrate ($n = 1.52$) and excited with TM-polarized light. The denomination of $\parallel$ or $\perp$ refers to the direction of the dipole with respect to the plane defined by the layer surface. The calculation is done analytically, using a recursive transfer matrix approach.[1] By virtue of reciprocity,[1,44] this pattern also corresponds to the radiation pattern of the dipole (when considering only the dominant TM-polarized emission). The critical angle of total internal reflection and the angle of excitation of SPPs at the air/gold interface are indicated by small arrows (41.1 and 43.5°, respectively). The excitation (and re-emission) pattern for the perpendicular case is invariant upon rotation around an axis normal to the interface (unlike the pattern for the parallel case). As a result, the peak emission pattern in the substrate forms the so-called *Kretschmann cone* in three dimensions; this is essential for the understanding of the collection/excitation efficiency in the Kretschmann configuration.

(i.e., whether the full Kretschmann cone is being collected, whether the excitation beam is fully coupled to the SPPs, etc). The enhancement factor in this configuration, accordingly, cannot be fully summarized as a single number, but rather it needs to be accompanied by a detailed specification of the excitation and collection optics configuration. It is interesting to note, for example, that the emission on the glass side is entirely funneled into a narrow angular cone; that is, provided the objective has a greater numerical aperture than the Kretschmann angle, all the radiation will be collected regardless of the particular NA of the objective.

Different Configurations for SPR and SERS. Four possible schemes are presented in Figure 2 that allow simultaneous SPR excitation and collection of SERS signals. Perhaps the most natural extension to the original Kretschmann scheme is shown in Figure 2a.[52,54,55] A laser beam couples to SPPs using the original Kretschmann excitation scheme with a glass prism. The SERS signal is collected from the air side with an objective in close proximity to the surface.[52] This excitation scheme precludes tight focusing as the physical presence of the prism limits the use of high-NA objectives. Further, the collection of the Raman signal from the air side misses the additional enhancement mechanism of the scattering process in the Kretschmann cone, situated on the opposite side. This is partially compensated though by the fact that a big fraction of the emission can be collected with a high numerical aperture from the air side (see Figure 1). The main difficulty with this scheme, besides the fact

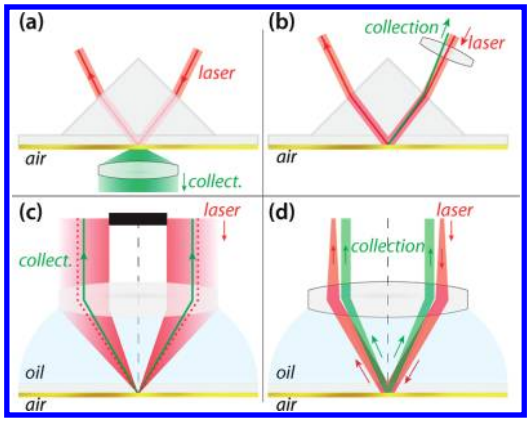

Figure 2. Diagrams of experimental schemes combining SPR and SERS spectroscopy in the Kretschmann configuration. The laser light is represented in red, the Raman-shifted radiation in green. (a) Prism coupling of a laser beam, and collection of the Raman-scattered light from the air side.[52] (b) Prism coupling and collection from the prism side using a long-distance low-to-medium NA objective.[35] (c) The incident beam is expanded to fill the objective, and the central part of the illumination cone is blocked.[53] The Raman signal is collected in backscattering from the same objective. (d) Schematic of the setup proposed in this paper. A shifted laser beam traverses off-axis an oil-immersion objective, and illuminates the gold film as a parallel beam. The Raman signal is collected through the same objective. In (b−d), the minute angular shift between excitation and collection produced by the dispersion of the resonance (typically ∼1°) is exaggerated for clarity.

that it requires a nonconventional excitation/collection configuration, is to ensure that the excitation spot is centered with the collection objective, especially for simultaneous measurement of the angular-dependent reflectivity and SERS. In fact, a large fraction of the work on SERS in the Kretschmann configuration has been based on nonconventional excitation/collection configurations. In contrast, the schematic proposed in Figure 2b collects the SERS signal from the prism side, in the more standard and much more convenient backscattering configuration.[35] Again, the presence of the prism imposes constraints on the objective that may be used; in particular only a small fraction of the Kretschmann cone of emitted Raman radiation is collected. For the same reason, microscopy cannot be carried out with this setup. Along these lines, it is worth highlighting the development of the so-called Weierstrass prism,[56−59] which allowed collection of the entire Kretschmann cone on the prism side.

The setups presented in Figure 2c,d, also based on a backscattering configuration, are more suitable for microscopy, using a high-numerical aperture oil-immersion objective in place of the glass prism to reach the angle of incidence corresponding to the excitation of SPPs. In Figure 2c (after ref 53, where such an approach was used for fluorescence, but not SERS, measurements), an expanded laser beam fills the back aperture of the objective and is tightly focused onto the substrate. A (small) portion of the beam couples to SPPs, and the SERS signal is collected in backscattering using the same objective. To restrict the range of incident angles and avoid undesirable heating of the metal substrate at high incident power, the central portion of the incident beam may be blocked. This setup has the problem that the spread of incident angles for coupling cannot be controlled very well, and the resulting poor coupling to SPPs prevents the simultaneous measurement of the SPR reflectivity (it also dramatically reduces SERS intensities, but this could in principle be compensated by a higher laser power). Finally, Figure 2d depicts the original scheme proposed in this paper, which is similar to one of the possible TIRF configurations[60] and to the scheme used for SPR microscopy.[61] It can be seen as a hybrid setup between those in Figure 2b,c, where an off-center incident beam enters a high-NA oil-immersion objective, also used for efficient collection of the SERS signals. This approach presents several advantages, including: (*i*) It is based on the convenient backscattering configuration and can therefore be implemented in most Raman microscopes with only minor modifications; (*ii*) The high NA objective in principle allows for a high spatial resolution for either spectroscopy or imaging of the collected light; (*iii*) The entire Kretschmann cone is collected, thereby maximizing the SERS signal; (*iv*) As will be shown in this work, it is possible under appropriate conditions to couple efficiently to SPPs and therefore carry out simultaneous measurements of the SPR reflectivity.

In this work, we will analyze in detail the technical aspects of this implementation, with a particular emphasis on the factors determining spot-size, coupling efficiency to SPPs, and spatial resolution, and will also demonstrate its efficacy on specific examples.

RESULTS AND ANALYSIS

Experimental Setup. Figure 3 presents in more details the experimental setup of Figure 2d that was developed to combine most efficiently standard microscopic SERS measurements with a Kretschmann excitation scheme in the backscattering configuration. Using a high-NA objective, the full Kretschmann cone of emitted radiation can be collected for all incident angles. This is, by itself, an important improvement of this setup compared to conventional backscattering prism-based coupling versions of the Kretschmann configuration for SERS.[35] Also, as a result, the enhancement factor due to the reemission (Raman) process was constant in our experiments and the angular dependence is therefore dictated by the local field enhancement (for excitation) only, that is, $\propto|E_{Loc}|^2/|E_0|^2$. Spatial resolution was achieved through the use of a standard optical microscope mounted with a high-NA objective (Olympus, Apo N, ×60, NA = 1.49, oil immersion) with standard specifications for Total Internal Reflection Fluorescence (TIRF) microscopy. Coupling of the incident laser to the surface mode was achieved by shifting the beam using a slanted glass cube (see Figure 3), whereby the beam emerges from the objective at a specific angle. The Supporting Information (SI) to the paper provides further experimental and theoretical details on the connection between the cube's angle and the angle of incidence on the sample. To optimize the coupling to the resonance, a collimated beam is required. To this end, a back-focal plane (BFP) lens (focal length 400 mm) was placed before the entrance of the microscope.[62] The exact position of this lens is crucial and was finely adjusted by observing the condition of minimum divergence of the beam (being transmitted through a transparent substrate like glass) in the far-field after the objective.

We have performed multiple characterizations of the experimental setup on known substrates and found good agreement with the corresponding theoretical expectations. In the SI we provide experimental plots for the angle-dependent reflectivity of both glass slides and thin metal films (control samples). The good collimation of the beam was assessed by the angular scan of the reflectivity in the Kretschmann configuration (TM-polarization).

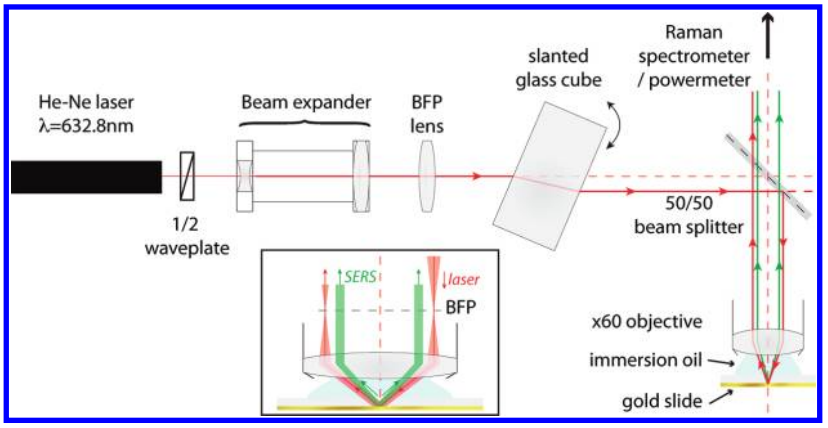

Figure 3. Schematic representation of the experimental setup. A He−Ne laser beam (λ = 632.8 nm) is directed toward the sample through the oil-immersion TIRF objective of a microscope. The direction of the linear polarization of the laser beam is adjusted with a half-wave plate. The beam is then expanded, and directed toward a convergent lens with focal distance f = 400 mm that is used to focus the beam onto the back-focal plane (BFP) of the microscope objective, thereby producing a collimated (parallel) beam when it reaches the sample. A glass cube is placed onto a motorized rotating stage, which enables a parallel displacement of the beam when it enters the microscope. As a result, the ray exits the objective at an angle directly related to the cube's rotation. The SI to the paper contains further details on the calibration of the cube rotation and its connection to the incident angle on the sample. The SERS signal, and the reflectivity (assessing the coupling to SPPs) are both monitored in backscattering through the beam splitter, as indicated in the figure. For clarity and display purposes only the laser light is shown in red, and the Raman light (to be collected) in green. Note that the minute displacement between the Raman and laser light (produced by the dispersion of the resonance) has been exaggerated. Inset: detailed view of the light beam near the microscope objective. The beam converges at the back-focal plane, and emerges collimated at the sample.

With gold substrates, better than 95% coupling was achieved, measured from the highest-to-lowest reflectivity values, and a resonance width comparable with the theoretical prediction.

Nile Blue (NB) molecules were deposited onto the metal surface, as in ref 35, and Raman spectra were measured using the backscattering configuration of Figure 3, with the simultaneous acquisition of reflectivity data. The results of this experiment are summarized in Figure 4 against the theoretical predictions. For each angle of incidence, a SERS spectrum was recorded (raw data shown in SI). The intensity of the 595 cm^{-1} peak of NB is plotted in Figure 4a, as a measure of the angular variation of the SERS enhancement factor. A clear correlation is observed between the sharp resonance in the SERS intensity and the coupling to the plasmon resonance directly monitored in the reflectivity (Figure 4b). As the incident angle reaches the optimum coupling condition, the incident light is converted to SPPs, visible as a dip in reflectivity, and the electromagnetic field in the vicinity of the Raman molecules is enhanced (Figure 1). The response is in good agreement with the theoretical predictions for this system, shown in Figure 4c,d.

The setup presented in Figure 3 uses a back-focal plane lens to realize a collimated beam incident on the sample, a crucial condition to achieve optimum coupling to SPPs, together with high local field enhancement factors. We now examine in detail the convoluted effects of beam divergence and spot size on the resonant coupling to SPP and the spatial resolution. This is clearly a crucial aspect for both SPR microscopy and SERS in the Kretschmann configuration, but the following discussion is in fact more general, and would indeed apply to any SPR experiments.

Trade-off between Spot Size and Coupling to SPPs. An ideal plane wave impinging on a thin metal film in the Kretschmann configuration can undergo total absorption at the exact angle of incidence corresponding to the SPP resonance. A real laser beam, however, conveys an intrinsic spread of angles that varies with the beam size, thus, impairing this ideal coupling. In turn, the beam

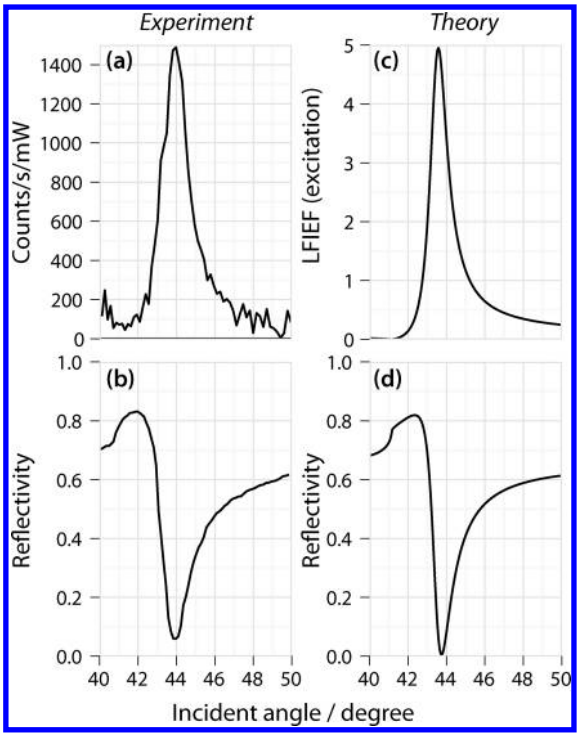

Figure 4. Experimental (left) and theoretical (right) variation of the reflectivity (bottom) and SERS intensity (top). Note that the SERS intensity follows, as expected, the angular dependence of the local field intensity EF (LFIEF). The calculation considers the following parameters derived from the experimental conditions: λ = 632.8 nm, 48 nm gold film with a 2 nm Ti adhesion layer, immersion oil with refractive index 1.52, dipole parallel to the interface. Plane wave illumination is assumed, with TM polarization. The films are commercially available from Ssens (www.ssens.nl, The Netherlands). The experimental signals were homogeneous over the sample as tested by measurements on 5−10 different points on the substrate.

dx.doi.org/10.1021/jp2107507 |J. Phys. Chem. A 2012, 116, 1000–1007

size is a crucial parameter in many applications, as it dictates the power density reaching the analyte for a given input power and may also be constrained to manage the spatial resolution. Indeed, in many microscopy applications in spectroscopy, the spatial resolution is primarily determined by the spot size (i.e., by the spatial resolution in excitation). It should however be noted that spatial filtering can also be carried out in the collection part of the system, by limiting the area of the sample image that is spectrally analyzed using slits or pinholes (in fact, many imaging techniques essentially do this in parallel by projecting the image on a CCD array). The spatial resolution is then dictated by the resolving power of the microscope objective; in our case (high NA objective), it is therefore in principle diffraction-limited. This approach is, however, not very efficient, in particular, if the spot size is much larger than the desired spatial resolution. Therefore, although microscopy with high spatial resolution is always possible in collection in our proposed setup owing to the high-NA objective, a small spot size is clearly desirable to improve the overall efficiency and simplify the setup.

At the same time a high degree of collimation is also required for the exciting beam, because of the narrow angular spread of the SPP resonance. Any divergence beyond typically one degree would result in part of the beam not coupling to SPPs, again reducing the efficiency. Unfortunately, from basic optics theory, spot size, and beam divergence are intrinsically anticorrelated and it cannot be varied independently (at least without losing laser power in the process). There is therefore an unavoidable trade-off between the spot size and the coupling to SPPs and this needs to be well understood to decide on the best strategy for a given desired spatial resolution in SPR/SERS microscopy. As we now show, our proposed setup is very flexible in this regard thanks to the beam expander used in excitation.

Figure 5 shows a simplified schematic of the excitation path of the beam, where we have included only the essentials. The beam increases to a diameter D after the expander, impinges onto the BFP lens, and is shifted off-center by the slanted glass cube. The lens focuses the beam onto the back focal plane of the objective, whereupon it emerges as a parallel beam with an angle (the resonance Kretschmann angle) onto the sample with a cross-sectional area, equivalent to spot size, at normal incidence, S. As is evident from Figure 5, in the ray optics description of the excitation path (which applies for the relatively large spot sizes considered here), the spot size S is directly proportional to the beam size D after the expander. Hence, a reduction in the excitation beam diameter (obtained by changing or removing the expander) yields a concomitant reduction in spot size until diffraction effects become important at small sizes (of the order of a micrometer-sized spot). Within the ray optics approximation, the rays reaching the sample should be parallel and inclined at the Kretschmann excitation angle (optimum coupling to SPPs), but as mentioned already, this is no longer the case for small spot sizes. A combination of perfectly collinear plane waves *cannot* describe a beam with finite spatial extent; instead, one must consider a continuous distribution of plane waves with slightly diverging wave vectors. In the approximation of large enough beam diameter, this corresponds to a bundle of light rays with a slight spread of angles around the mean beam direction (given by the Kretschmann angle). In the next subsection, we use a simple model to assess the trade-off between spatial resolution and coupling, and we compare it with direct experimental results in our system.

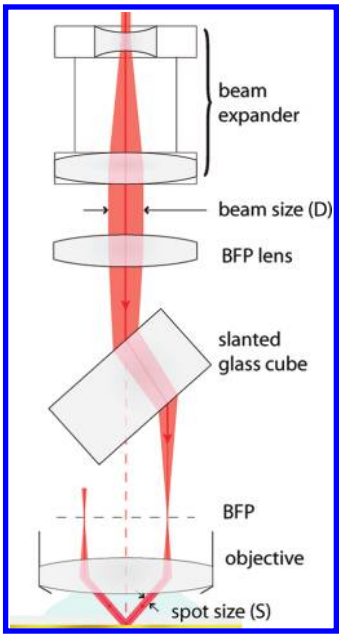

Figure 5. Simplified optical layout illustrating the ray-optics approximation of the beam (not to scale for clarity). The spot size (S) is directly proportional to the diameter (D) of the off-axis beam feeding the Back Focal Plane (BFP) lens after the expander. If the ray optics picture were valid all the way to very small beam sizes ($\sim\lambda$), we could potentially create a very small spot size S by reducing D as much as possible, and still achieve a very good coupling to SPPs with a parallel beam. This does *not* happen in reality because the smaller the beam size the more evident it becomes that it has a natural (unavoidable) divergence. In fact, the product of the beam size with the beam divergence (*étendue*) cannot be made smaller than its original value characterizing the laser beam. Accordingly, a small spot is always associated with some degree of spread in the incidence angles on the sample and, therefore, a worsening of the coupling conditions to SPPs.

Accounting for the Beam Divergence. We can use a simplified theory to account for the beam-like aspects of the excitation that still uses the ray-optics description but explicitly allows for a spread of incident angles. When the mean angle is at resonance, part of the beam is slightly off-resonance, thus leading to a residual reflectivity and a broadening of the reflectivity dispersion curve. To evaluate the detrimental effect of reducing the beam size on its coupling to SPPs, we follow here the approach proposed by Villatoro and co-workers.[63] The incident laser beam is modeled as a Gaussian beam of waist radius w_0 (corresponding to the half-width at $1/e^2$). After traversing off-axis the objective, the intensity profile $I(x',y')$ suffers a compression along the y' direction

$$I(x',y') = I_0 \exp\left(-2\frac{x'^2}{w_0^2}\right) \exp\left(-2\frac{y'^2}{w'^2_0}\right) \quad (1)$$

with $w'_0 = w_0 \cos\theta_i$, where θ_i is the angle of the incident beam ($\sim$45° at the SPP resonance) relative to the normal. The effective response G ($G \equiv |r|^2$ for the reflectivity, or $G \equiv$ local field intensity EF) can be obtained as an average over the response of a spectrum of individual plane waves, weighted by a Gaussian distribution of incident angles θ centered around the average

angle θ_i,

$$G(\theta_i) = \frac{kw'_0}{\sqrt{2\pi}} \int_{-\infty}^{\infty} G(\theta) \exp\left(-\frac{k^2 w'^2_0}{2} (\theta_i - \theta)^2 \right) d\theta \quad (2)$$

where $k = 2\pi n/\lambda$ is the wavevector in the oil immersion medium of refractive index n = 1.52. The results of this averaging are shown in Figure 6 for varying beam waist radii and show a clear broadening of the sharp spectral features associated with the plasmon resonance and the critical angle of total internal reflection.

Experimentally, the beam size was varied by removing the beam-expander in Figure 3. The beam size reaching the sample was measured at normal incidence, using a knife-edge technique (see the SI of ref 23) to extract the beam waist radius w_0. This comparison is presented in Figure 6a,b, with two different spot sizes (radius of the spots: ∼3 and ∼15 μm). As can be appreciated from the figure, the smaller the spot size, the lower the efficiency of the SERS signal, when properly normalized by the incident power (in [counts·s^{-1}·mW^{-1}]). This is a direct consequence of the fact that, despite having the same collection efficiency in both cases, the coupling to SPPs is compromised when the spot size is reduced as described in the previous section. This is also revealed in the broadening of the resonance, which is narrower (better coupling) for the larger spot (less spread in incident angles).

Strategies for SPR/SERS Microscopy. The previous studies demonstrate that there is an unavoidable trade-off between spot-size and beam divergence in SPR/SERS microscopy in general and in our proposed setup in particular. If the beam divergence is reduced to maximize coupling to SPPs, then the minimum spot-size is limited to about ∼15−20 μm with gold substrates (the situation is considerably worse for silver, ∼300 μm for optimum coupling, owing to its narrower SPR response[63]). If the spot-size is reduced to about ∼5 μm diameter, then the best achievable coupling to SPP is of the order of 30−35% only. Which combination of spot-size/beam divergence is chosen therefore depends on the application. For example, if a spatial resolution of ∼15−20 μm is sufficient, and the input power density not critical, then one should use these relatively large spot sizes where the best coupling to SPP is obtained. In this latter case, the true angle-dependent SPR reflectivity can then be measured together with a large SERS intensity (since both excitation and emission are efficient here). Three alternative and arguably complementary strategies are possible to improve the spatial resolution:

- The imaging approach, which is based on projecting the sample image onto a CCD array, and is the basis for SPR microscopy. The main disadvantage here is that obtaining the SERS spectrum is difficult, although fluorescence intensity images (and possibly integrated SERS intensities within a given spectral window) can in principle be obtained using spectral filters.
- Spatial filtering in collection, where only a small area of the image (defined by the use of pinholes) is spectrally analyzed. Both SPR reflectivity and SERS spectra can then be measured, but the efficiency of the process is not very good as the spot-size is larger, or much larger than the analyzed area. This could however be compensated by increased laser power, at the expense of overheating.

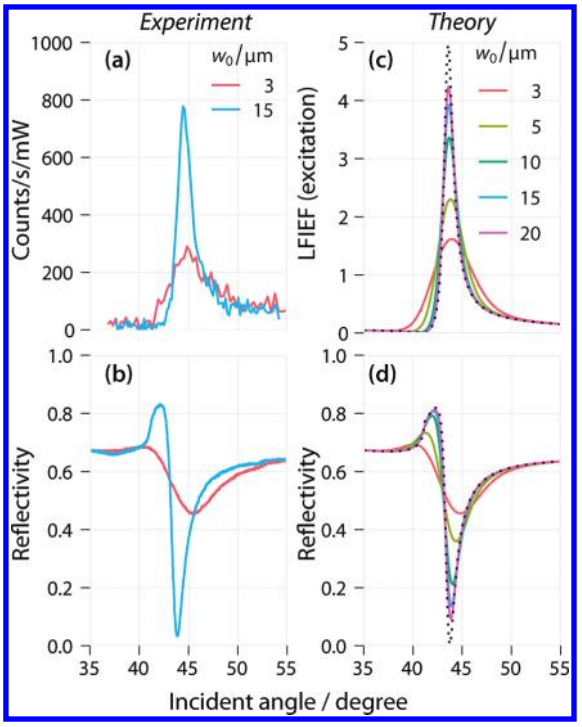

Figure 6. Influence of the beam size on the coupling efficiency. (a) Integrated Raman counts normalized by the integration time and incident laser power. (b) Experimental reflectivity curves for the same configuration, normalized by the maximum value of the corresponding theoretical predictions. The beam waist radii corresponding to the two different experimental configurations were measured as 15 μm (beam expander), and 3 μm (no beam expander). (c) Theoretical local field intensity enhancement factor (LFIEF) for a dipole parallel to the interface and (d) reflectivity curves for the same configuration. The model considers a 48 nm Au film (with 2 nm Ti adhesion layer) illuminated in the Kretschmann configuration (λ = 632.8 nm, refractive index of the prism 1.52). The beam waist radius W_0 is varied from 3 to 20 μm. In dashed lines is shown the solution for plane wave illumination (which achieves the best coupling condition).

- Spot size reduction: in this case, the power density illuminating the area of interest is much larger (potentially providing a large SERS signal), but this is partly compensated by the fact that coupling to SPPs is reduced. The latter may also prevent a clear measurement of the SPR reflectivity minimum. This approach may therefore be suited to SERS measurements on flat surfaces (which still benefits from the collection of the entire Kretschmann cone), but is not appropriate to combined SPR/SERS microscopy studies.

The exact strategy (or strategies, since combining them could be advantageous in some cases) should be decided on a case-by-case basis. This brief discussion however highlights the importance of being able to adjust spot-size/beam divergence at will in such experiments. This flexibility is therefore an important feature of our proposed setup.

Platform for Analytical SERS Studies. The standard implementation of the Kretschmann configuration with a prism can only achieve a very good coupling to SPPs in some specific circumstances that do not involve high magnification objectives.[35] Furthermore, due to the tilted substrate, it is not possible to scan over the surface of the sample without compromising the focusing condition. In contrast, the coupling scheme

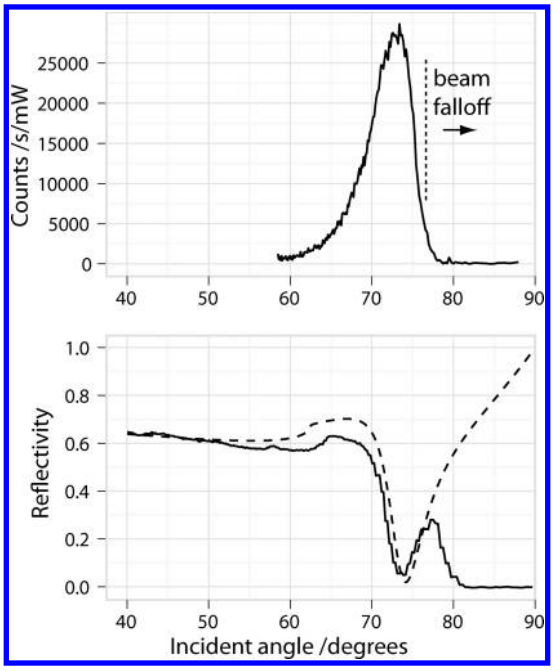

Figure 7. Experimental variation of the reflectivity (bottom) and integrated 595 cm^{-1} Raman peak of Nile Blue (top). A 5:1 beam expander was used to expand the laser beam of wavelength $\lambda = 632.8$ nm. The substrate consisted in a 48 nm gold film with a 2 nm Ti adhesion layer deposited onto a glass substrate with refractive index 1.52. The gold surface was exposed to Nile Blue molecules dispersed in water with concentration 100 μM. The theoretical prediction for the reflectivity is shown with a dashed line. The experiment follows closely the theory until the off-axis beam approaches the edge of the objective, resulting in a beam falloff. The Kretschmann resonance in water is at a very high incidence angle of ~74°, but still achievable with an objective with NA = 1.49, like the one used in our setup.

proposed in this paper offers a real promise of performing SERS microscopy in a convenient platform for analytical studies. Where the use of a prism imposes a natural limitation on how close one can approach the sample, forcing the use of long working distance, low-NA objectives, our SPR configuration uses a conventional TIRF illumination scheme suitable for microscopy with high-NA and high-magnification objectives. In terms of performance, only a small fraction of the emitted Kretschmann cone containing the SERS signal from the substrate is collected in the case of prism-coupling. This has been discussed extensively in ref.[35] Comparatively, the present configuration collects the *full* Kretschmann cone in emission.

To illustrate the potential of the proposed configuration to perform applications-driven analytical studies, we present in Figure 7 a proof-of-principle measurement of the reflectivity and Raman resonance of Nile Blue molecules immersed in *water*. This is a situation highly relevant to a number of applications, such as biosensing, where working in air is a disadvantage. In a liquid solvent, molecules can flow in the solution; notably it allows the study of fluorescence enhancement which would be mostly quenched in the first layer as studied in dry conditions. The plasmon resonance for the glass/gold/water system is centered around ~74°, close to the limit of the maximum angle allowed by the high NA objective. The high, almost grazing angle, together with the relatively "large" beam diameter, results in a sharp drop of the signal when approaching ~80°. Nevertheless, the SPR position is clearly observed in the reflectivity curve, and the Raman signal follows the expected angular resonance until the loss of incident light causes a sharp drop in signal. These results confirm the potential of hybrid SPR-SERS microscopy in a broad range of analytical applications, that might include substrates in air or in water with improved spatial resolution over large areas of uniform enhancement.

CONCLUSION AND OUTLOOK

This paper presents a new way of performing SERS. By combining aspects of Raman microscopy with a typical setup used in SPR microscopy, we achieved an analytical instrument that is capable of performing SERS microscopy over flat surfaces. The main characteristics of this new way of doing SERS are (*i*) a good spatial resolution through the use of a high-NA objective, (*ii*) improved collection efficiency with respect to typical prism-coupling versions of the Kretschmann configuration, (*iii*) uniform enhancement over the surface, and (*iv*) the ability to simultaneously measure the SPR reflectivity. Besides the obvious study of heterogeneous monolayers on surfaces (due to the orientation of domains of molecules, or otherwise), it is possible to envision future applications with functionalized surfaces where hundreds (or possibly thousands) of compounds could be monitored on a single SPR-chip with perfectly uniform enhancement, using the ability to spatially resolve the signals at different places on the surface. Last, but not least, this technique sets the necessary platform to attempt single-molecule detection on flat surfaces. The spatial resolution feature is essential in this latter case. As pointed out in the introduction, this technique does not involve any new development in the nanotechnology of the substrates (which might be difficult to replicate and exploit), but rather it is an instrumental development in the way SPPs are excited and the SERS signal collected. It is interesting to realize that since the pioneering work on the coupling of SPPs by Kretschmann,[22] Otto,[64] and Raether[65] in the late 60s and early 70s, the technique of SERS is only now being pursued in conjunction with microscopy and excitation of surface plasmons on planar substrates[52,54,55] (which has requirements of its own in terms of spot size and collection of the signal). While there are natural limitations to satisfy the requirements of SERS microscopy, it is clear from the results in this paper that the two techniques can work in a fruitful symbiosis, opening new doors to the applications and use of SERS as an analytical technique.

ASSOCIATED CONTENT

Supporting Information. Reflectivity curves on glass and gold substrates; angular resonance of the NB Raman spectra; and relation between the cube angle and the angle of incidence. This material is available free of charge via the Internet at http://pubs.acs.org.

REFERENCES

(1) Le Ru, E. C.; Etchegoin, P. G. *Principles of Surface Enhanced Raman Spectroscopy and Related Plasmonic Effects*; Elsevier: Amsterdam, 2009.

(2) Aroca, R. F. *Surface-Enhanced Vibrational Spectroscopy*; John Wiley and Sons: Chichester, 2006.

(3) Green, M.; Liu, F. M. *J. Phys. Chem. B* **2003**, *107*, 13015–13021.

(4) Dieringer, J. A.; McFarland, A. D.; Shah, N. C.; Stuart, D. A.; Whitney, A. V.; Yonzon, C. R.; Young, M. A.; Zhang, X.; Duyne, R. P. V. *Faraday Discuss.* **2006**, *132*, 9–26.

(5) Perney, N. M. B.; Baumberg, J. J.; Zoorob, M. E.; Charlton, M. D. B.; Mahnkopf, S.; Netti, C. M. *Opt. Express* **2006**, *14*, 847–857.
(6) Drachev, V. P.; Thoreson, M. D.; Nashine, V.; Khaliullin, E. N.; Ben-Amotz, D.; Davisson, V. J.; Shalaev, V. M. *J. Raman Spectrosc.* **2005**, *36*, 648–656.
(7) Vlckova, B.; Moskovits, M.; Pavel, I.; Siskova, K.; Sladkova, M.; Slouf, M. *Chem. Phys. Lett.* **2008**, *455*, 131–134.
(8) Jackson, J. B.; Westcott, S. L.; Hirsch, L. R.; West, J. L.; Halas, N. J. *Appl. Phys. Lett.* **2003**, *82*, 257–259.
(9) Hu, J.; Zhao, B.; Xu, W.; Fan, Y.; Li, B.; Ozaki, Y. *Langmuir* **2002**, *18*, 6839–6844.
(10) Fan, M.; Brolo, A. G. *Phys. Chem. Chem. Phys.* **2009**, *11*, 7381–7389.
(11) Nehl, C. L.; Liao, H.; Hafner, J. H. *Nano Lett.* **2006**, *6*, 683–688.
(12) Graham, D.; Thompson, D. G.; Smith, W. E.; Faulds, K. *Nat. Nanotechnol.* **2008**, *3*, 548–551.
(13) Taylor, R. W.; Lee, T.-C.; Scherman, O. A.; Esteban, R.; Aizpurua, J.; Huang, F. M.; Baumberg, J. J.; Mahajan, S. *ACS Nano* **2011**, *5*, 3878–3887.
(14) Le Ru, E. C.; Etchegoin, P. G.; Grand, J.; Félidj, N.; Aubard, J.; Lévi, G.; Hohenau, A.; Krenn, J. *Curr. Appl. Phys.* **2008**, *8*, 467–470.
(15) Sawai, Y.; Takimoto, B.; Nabika, H.; Ajito, K.; Murakoshi, K. *J. Am. Chem. Soc.* **2007**, *129*, 1658–1662.
(16) Wang, H.; Brandl, D. W.; Le, F.; Nordlander, P.; Halas, N. J. *Nano Lett.* **2006**, *6*, 827–832.
(17) Steidtner, J.; Pettinger, B. *Phys. Rev. Lett.* **2008**, *100*, 236101–(1−4).
(18) Pettinger, B.; Picardi, G.; Schuster, R.; Ertl, G. *Single Mol.* **2002**, *5*−*6*, 285–294.
(19) Pettinger, B. *Mol. Phys.* **2010**, *108*, 2039–2059.
(20) Maier, S. A. *Plasmonics, Fundamentals and Applications*; Springer: Berlin, 2007.
(21) Novotny, L.; Hecht, B. *Principles of Nano-Optics*; Cambridge University Press: Cambridge, 2006.
(22) Kretschmann, E. *Z. Phys.* **1971**, *241*, 313–324.
(23) Le Ru, E. C.; Blackie, E.; Meyer, M.; Etchegoin, P. G. *J. Phys. Chem. C* **2007**, *111*, 13794–13803.
(24) Kleinman, S. L.; Ringe, E.; Valley, N.; Wustholz, K. L.; Phillips, E.; Scheidt, K. A.; Schatz, G. C.; Van Duyne, R. P. *J. Am. Chem. Soc.* **2011**, *133*, 4115–4122.
(25) Blackie, E.; Le Ru, E. C.; Meyer, M.; Timmer, M.; Burkett, B.; Northcote, P.; Etchegoin, P. G. *Phys. Chem. Chem. Phys.* **2008**, *10*, 4069–4200.
(26) Etchegoin, P. G.; Le Ru, E. C. *Anal. Chem.* **2010**, *82*, 2888–2892.
(27) Stranahan, S. M.; Willets, K. A. *Nano Lett.* **2010**, *10*, 3777–3784.
(28) Cortés, E.; Etchegoin, P. G.; Le Ru, E. C.; Fainstein, A.; Vela, M.; Salvarezza, R. *J. Am. Chem. Soc.* **2010**, *132*, 18034–18037.
(29) dos Santos, D. P.; Andrade, G. F.; Temperini, M. L. A.; Brolo, A. G. *J. Phys. Chem. C* **2009**, *113*, 17737–17744.
(30) Ward, D. R.; Halas, N. J.; Ciszek, J. W.; Tour, J. M.; Wu, Y.; Nordlander, P.; Natelson, D. *Nano Lett.* **2008**, *8*, 919.
(31) Etchegoin, P. G.; Meyer, M.; Blackie, E.; Le Ru, E. C. *Anal. Chem.* **2007**, *79*, 8411–8515.
(32) Etchegoin, P. G.; Le Ru, E. C. *Phys. Chem. Chem. Phys.* **2008**, *10*, 6079–6089.
(33) Le Ru, E. C.; Grand, J.; Sow, I.; Somerville, W. R. C.; Etchegoin, P. G.; Treguer-Delapierre, M.; Charron, G.; Félidj, N.; Lévi, G.; Aubard, J. *Nano Lett.*
(34) Natan, M. J. *Faraday Discuss.* **2006**, *132*, 321–328.
(35) Meyer, S. A.; Le Ru, E. C.; Etchegoin, P. G. *Anal. Chem.* **2011**, *83*, 2337–2344.
(36) Stokes, R. J.; Macaskill, A.; Dougan, J. A.; Hargreaves, P. G.; Stanford, H. M.; Smith, W. E.; Faulds, K.; Graham, D. *Chem. Commun.* **2007**, *27*, 2811–2813.
(37) Alexander, T. A.; Le, D. M. *Appl. Opt.* **2007**, *46*, 3878–3890.
(38) Shim, S.; Stuart, C. M.; Mathies, R. A. *ChemPhysChem* **2008**, *9*, 697–699.
(39) Meyer, S. A.; Le Ru, E. C.; Etchegoin, P. G. *J. Phys. Chem. A* **2010**, *114*, 5515.
(40) Moskovits, M. *J. Chem. Phys.* **1982**, *77*, 4408.
(41) Le Ru, E. C.; Meyer, S. A.; Artur, C.; Etchegoin, P. G.; Grand, J.; Lang, P.; Maurel, F. *Chem. Commun.* **2011**, *47*, 3903–3905.
(42) Otto, A. In *Surface-Enhanced Raman Scattering: Classical and Chemical Origins*;Cardona, M., Gütherodt, G., Eds.; Springer-Verlag: Berlin, 1984.
(43) Etchegoin, P. G.; Le Ru, E. C.; Meyer, M. *J. Chem. Phys.* **2006**, *125*, 164705−1–3.
(44) Le Ru, E. C.; Etchegoin, P. G. *Chem. Phys. Lett.* **2006**, *423*, 63–66.
(45) Huang, B.; Yu, F.; Zare, R. N. *Anal. Chem.* **2007**, *79*, 2979–2983.
(46) Axelrod, D. *Methods Enzymol.* **2003**, *361*, 1–33.
(47) O′Shannessy, D. J. *Curr. Opin. Biotechnol.* **1994**, *5*, 65–71.
(48) Malmqvist, M. *Curr. Opin. Immunol.* **1993**, *5*, 282–286.
(49) Szabo, A.; Stolz, L.; Granzow, R. *Curr. Opin. Struct. Biol.* **1995**, *5*, 699–705.
(50) Fisher, R. J.; Fivash, M. *Curr. Opin. Biotechnol.* **1994**, *5*, 389.
(51) Margulies, D. H.; Plaksin, D.; Khilko, S.; Jelonek, M. T. *Curr. Opin. Immunol.* **1996**, *8*, 262–270.
(52) Liu, Y.; Xu, S.; Tang, B.; Wang, Y.; Zhou, J.; Zheng, X.; Zhao, B.; Xu, W. *Rev. Sci. Instrum.* **2010**, *81*, 036105−1–036105−3.
(53) Stefani, F. D.; Vasilev, K.; Bocchio, N.; Stoyanova, N.; Kreiter, M. *Phys. Rev. Lett.* **2005**, *94*, 023005.
(54) Liu, Y.; Xu, S.; Xuyang, X.; Zhao, B.; Xu, W. *J. Phys. Chem. Lett.* **2011**, *2*, 2218–2222.
(55) Liu, Y.; Xu, S.; Li, H.; Jian, X.; Xu, W. *Chem. Commun.* **2011**, *47*, 3784–3786.
(56) Wittke, W.; Hatta, A.; Otto, A. *Appl. Phys. A* **1989**, *48*, 298–294.
(57) Futamata, M. *Langmuir* **1995**, *11*, 3894–3901.
(58) Futamata, M.; Keim, E.; Bruckbauer, A.; Schumacher, D.; Otto, A. *Appl. Surf. Sci.* **1996**, *100/101*, 60–63.
(59) Futamata, M. *Appl. Opt.* **1997**, *36*, 364–375.
(60) Axelrod, D. In *Optical Imaging and Microscopy, Springer Series in Optical Sciences*; Török, P., Kao, F. J., Eds.; Springer Verlag: Berlin, 2007.
(61) Stefani, F. D.; Vasilev, K.; Bocchio, N.; Stoyanova, N.; Kreiter, M. *Phys. Rev. Lett.* **2005**, *94*, 023005.
(62) Huang, B.; Yu, F.; Zare, R. N. *Anal. Chem.* **2007**, *79*, 2979–2983.
(63) Villatoro, J.; Garcia-Valenzuela, A. *Appl. Opt.* **1999**, *38*, 4837–4844.
(64) Otto, A. *Z. Phys.* **1968**, *216*, 398–410.
(65) Kretschmann, E.; Raether, H. *Z. Naturforsch.* **1968**, *23A*, 2135–2136.

Supplementary Information for: "Combined SPR and SERS Microscopy in the Kretschmann Configuration"

Stefan A. Meyer, Baptiste Auguié, Eric C. Le Ru, and Pablo G. Etchegoin

The MacDiarmid Institute for Advanced Materials and Nanotechnology, School of Chemical and Physical Sciences, Victoria University of Wellington, P.O. Box 600, 6140 Wellington, New Zealand

(Dated: December 19, 2011)

Basic characterization of the SERS/SPR setup

In order to understand how the experimental setup behaves in controlled situations, we have performed basic reflectivity experiments on glass and gold in TM-polarisation. Figure S1 shows the reflectivity data as a function of angle of incidence θ_s for glass and gold, respectively. The specular reflectivity was measured in backscattering, as in Fig. 2 of the main paper. The figure also shows the theoretical expectation for the reflectivity in the different cases (dashed lines). As can be appreciated, the agreement between theory and experiment is quite satisfactory. Crucially, the region of total internal reflection for the glass/air interface (top panel, $\geq 42°$) presents a uniform reflectivity of unity, spanning the full range of the plasmon resonance (bottom panel). Immediately before the critical edge of total internal reflection, the Brewster angle for the glass/air interface ($\sim 33.3°$, top panel) is marked with minimum reflectivity close to 0, confirming the well-maintained TM-polarisation of the incident beam. A weak low-frequency noise can be noted, originating from spurious reflections in the optical elements. Wider angular scans (not shown) were also performed to verify that the reflectivity was symmetric for positive and negative values of θ_s, i.e. with the beam shifted to one side or the other from the axis.

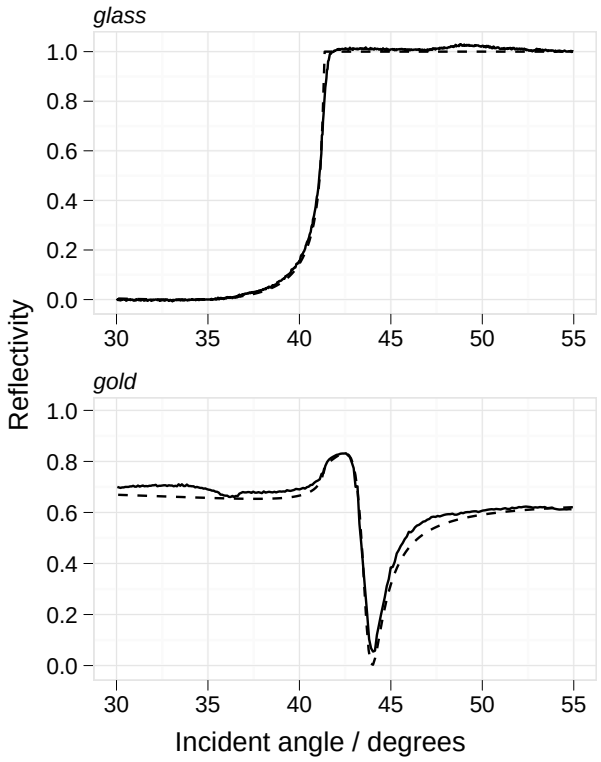

FIG. S1: Experimental (solid lines) and theoretical (dashed lines) TM-polarized reflectivities on glass (top) and gold (bottom) as a function of the incident (internal) angle (see Fig. S3 and Fig. 2 in the main paper). The experiment is done for an expanded beam (i.e. for a beam with a minimum divergence). The agreement between theory and experiment is very good and reveals that there is no spurious experimental distortion in the beam path.

Angular resonance of the NB Raman spectra

It is interesting to show the actual raw Raman data for the NB peak at 595 cm^{-1} across the resonance (as in Ref. [1]). Figure S2 presents the actual Raman data for one of the examples given in the paper, after substraction of the fluorescence background. A clear angular resonance is seen over the very small angular range 19°–20.5° (cube angle) corresponding to the Kretschmann resonance. The data were recorded as a time series sequence, synchronous with the scanning of the (shifter) cube (see Fig. 2 of the main paper).

Relation between the cube angle and the angle of incidence

The connection between the shifter cube angle and the incidence angle is mostly linear up to ~50° and was fully characterised by both measurements and calculation. The essential geometrical aspects of the problem that link the angle of rotation of the cube θ_c with the angle of incidence θ_s are displayed in Fig. S3(a). The mathematical connection between θ_c and θ_s is established through equations 1 and 2.

$$s = e \cdot \frac{\sin\left(\theta_c - \theta_c'\right)}{\cos\theta_c'}; \qquad \theta_c' = \arcsin\left(\sin\theta_c / n\right) \tag{1}$$

describes the parallel shift of the beam through a parallelepiped of refractive index $n = 1.5$ and thickness $e = 25.4\,\mathrm{mm}$. Abbe's sine condition provides the final link between the off-axis beam and the incident angle,

$$\theta_s = \arcsin\left(s/f\right) \tag{2}$$

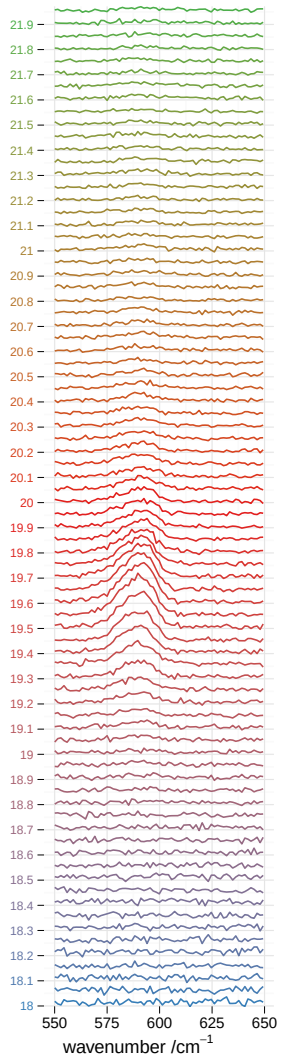

FIG. S2: Measured Raman spectra of Nile Blue molecules (595 cm^{-1} mode) adsorbed on a gold substrate (in air), illuminated at different incident angles (λ_L = 632.8 nm) in the Kretschmann configuration depicted in Fig. 2 (main paper). Spectra are shifted vertically for clarity. The Kretschmann resonance can be clearly seen within a very small angular range. The plots presented in the paper are always for the integrated intensity of the Raman peak across the resonance.

where, for our system, f = 4.2 mm is the effective focal length of the objective.

In Fig. S3(c) we show a plot of θ_s as a function of θ_c. As can be observed, the connection between the two is fairly linear up to $\theta_s \sim 50°$, where nonlinearity rapidly sets in. The Kretschmann resonance is observed around $\theta_s \sim 44°$ for 48 nm films of either Ag and Au in air (the resonance angle is fairly insensitive to thickness and wavelength [2]). The incidence angle can also be measured experimentally using a graduated scale on a dielectric cube, as depicted in the photo of Fig. S3(b). The experimental determination of the calibration of the angle of incidence is presented in Fig. S3(c) against the theoretical expectation. Excellent agreement between theory and experiment is observed, for an effective focal length f = 4.2 mm. Once determined, this value was fixed in the angular conversions. A slight offset of the origin was allowed to vary as a free parameter in order to match the observed plasmon resonance position with the theoretical predictions.

[1] Meyer, S. A.; Le Ru, E. C.; Etchegoin, P. G. *Anal. Chem.* **2011**, *83*, 2337–2344.

[2] Le Ru, E. C.; Etchegoin, P. G. *Principles of Surface Enhanced Raman Spectroscopy and Related Plasmonic Effects*; Elsevier: Amsterdam, 2009.

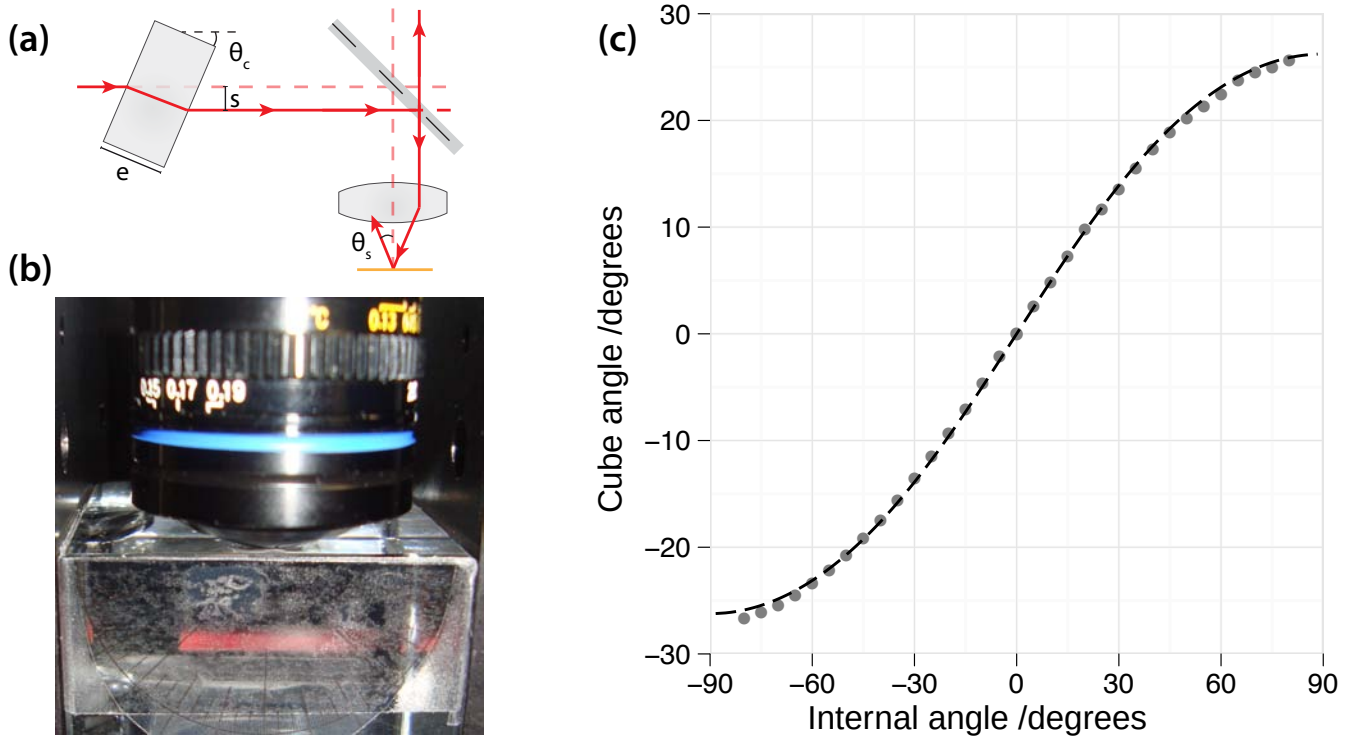

FIG. S3: (a) Schematic representation of the beam displacement used for the angle scan. A laser beam traverses a glass cube (refractive index 1.5) rotated by an angle θ_c and undergoes a parallel shift s. After being redirected by a beam-splitter, the shifted beam enters the microscope objective off-axis, and reaches the sample with an angle θ_s. (b) Photograph of the experimental apparatus used to measure the variation of incident angle vs. cube angle. A protractor printed on a transparency was glued onto a glass cube of refractive index 1.5 matching that of the oil immersion of the TIRF objective. By monitoring the position of the beam interesecting the angular marks along the edge of the cube, a reading of the incident angle was correlated with the computer-controlled rotation stage of the glass cube shifting the beam. (c) Measured (points) and predicted (dashed line) variation of the incident angle against the cube's angle. Negative angles refer to the beam incident from the other side of the normal.